

Comprehensive study of LIV in atmospheric and long-baseline experiments

Deepak Raikwal^{a,b} Sandhya Choubey,^{c,d} Monojit Ghosh,^e

^a*Harish-Chandra Research Institute, A CI of Homi Bhabha National Institute, Chhatnag Road, Jhansi, Prayagraj - 211019*

^b*Homi Bhabha National Institute, Anushakti Nagar, Mumbai 400094, India*

^c*Department of Physics, School of Engineering Sciences, KTH Royal Institute of Technology, AlbaNova University Center, Roslagstullsbacken 21, SE-106 91 Stockholm, Sweden*

^d*The Oskar Klein Centre, AlbaNova University Center, Roslagstullsbacken 21, SE-106 91 Stockholm, Sweden*

^e*Center of Excellence for Advanced Materials and Sensing Devices, Ruder Bošković Institute, 10000 Zagreb, Croatia*

E-mail: choubey@kth.se, mghosh@irb.hr, deepakraikwal@hri.res.in

ABSTRACT: In this paper we have presented a comprehensive study of Lorentz Invariance Violation (LIV) in the context of atmospheric neutrino experiment ICAL and long-baseline experiments T2HK and DUNE. Our study consists of the full parameter space of the LIV parameters (isotropic) i.e., six CPT violating LIV parameters ($a_{\alpha\beta}$) and six CPT conserving LIV parameters ($c_{\alpha\beta}$). In this study our objective is to calculate the upper bound on all the LIV parameters with respect to the individual experiments and their combination. Our results show that DUNE gives the best sensitivity for the parameters a_{ee} , $a_{e\mu}$, $a_{e\tau}$ and $a_{\mu\tau}$ in its 7 years of running whereas ICAL gives the best sensitivity on $a_{\mu\mu}$, $a_{\mu\tau}$, c_{ee} , $c_{\mu\mu}$, $c_{\tau\tau}$ and $c_{\mu\tau}$ in its 10 years of running. For $a_{\tau\tau}$, the sensitivity of DUNE and ICAL is similar. The combination of T2HK, DUNE and ICAL, gives the best sensitivity for $a_{e\mu}$ and a_{ee} with respect to all the existing bounds in the literature. For the CPT even diagonal parameters (isotropic) c_{ee} and $c_{\mu\mu}$, our work provides the first ever bounds.

Contents

1	Introduction	1
2	LIV and its effect on neutrino oscillation	3
3	Experimental configuration	4
3.1	ICAL detector at the INO facility	4
3.1.1	Detector	4
3.1.2	Flux	5
3.1.3	Event Generator	5
3.1.4	Binning Scheme	5
3.1.5	Systematic uncertainties	5
3.2	DUNE	6
3.3	T2HK	6
4	Discussion at the probability level	7
4.1	ICAL	7
4.2	DUNE	9
4.3	T2HK	12
5	Results	13
5.1	Sensitivity of $a_{\alpha\alpha}$	13
5.2	Sensitivity of $a_{\alpha\beta}$	15
5.3	Sensitivity of $c_{\alpha\alpha}$	16
5.4	Sensitivity of $c_{\alpha\beta}$	16
6	Comparison with previous results	19
7	Summary and conclusion	21

1 Introduction

Lorentz invariance is one of the fundamental principles of quantum field theory. However, it has been shown that one can have Lorentz invariance violation (LIV) in theories of quantum gravity at Planck scale ($M_P \sim 10^{19}$ GeV) [1]. In low energy theories, the effect of LIV is suppressed by M_P . The Standard Model of particle physics can be extended to include such LIV [2] and can be probed via three basic mechanisms: coherence, interference and extreme effects. The interference phenomenon of neutrino oscillation, in which active neutrinos oscillate among their flavors, provide a unique opportunity to probe the LIV effects. In the presence of LIV, the neutrino oscillation Hamiltonian gets modified and

therefore terms describing the LIV appear in the neutrino oscillation probabilities. The LIV parameters that appear in the neutrino oscillation probabilities can be either CPT violating or CPT conserving.

In this paper, we will present a comprehensive analysis of LIV in the context of upcoming long-baseline neutrino experiments T2HK [3] in Japan and DUNE [4] in USA and, upcoming atmospheric neutrino experiment ICAL [5] at the INO facility. In particular, we will study the capability of these experiments to put an upper bound on the parameters of LIV. Note that study of LIV in the context of DUNE and ICAL has been performed earlier. In what follows next, we will mention the studies that have been carried out in the past and the novel features in our work, which we will be showing for the very first time. In the context of DUNE, Ref. [6] obtained the upper bounds on the CPT violating LIV parameters and Ref. [7] studies the effect of LIV on the determination of the octant of atmospheric mixing angle θ_{23} and on the determination of the leptonic phase δ_{CP} . A combined bound on the CPT violating LIV parameters for DUNE and the long-baseline experiment option at KM3NeT [8] namely P2O [9] has been obtained in Ref. [10]. For ICAL, Ref [11] calculated bounds on the three off-diagonal of CPT violating LIV parameters taking a energy window of the neutrinos to be 1 GeV to 25 GeV with an assumption that the phases which are associated with the LIV parameters have less than 1% effect on the results. To the best of our knowledge, study of LIV in the context of T2HK has not been performed in the past¹. Apart from T2HK, DUNE and ICAL, LIV has been studied in the context of Super-Kamiokande [14], IceCube [15, 16], T2K and NO ν A [17–19]. In this present work, we aim to perform a detailed study of LIV in the context of T2HK, DUNE and ICAL and compare our results with the existing bounds on the LIV parameters. In our study, we will consider the complete LIV parameter space: namely six CPT conserving LIV parameters and six CPT violating LIV parameters. In addition, for ICAL we will consider an energy range up to 100 GeV and consider the full effect of the phases associated with the parameters of LIV. We will show in our work that an analysis with atmospheric neutrinos with a higher energy range provide better results as the parameters of LIV are more sensitive in the higher energy region. Further, our results will also show that the phases associated with the LIV parameters have a non-trivial effect on the final results in ICAL. Apart from the individual sensitivities of each experiment, we will also show the combined sensitivity of these three experiments. Therefore for the very first time our work demonstrates: (i) study of LIV in the context of T2HK, (ii) study of CPT conserving LIV parameters in the context of DUNE and ICAL, (iii) analysis of the diagonal CPT violating LIV parameters in the context of ICAL, (iv) study of LIV with an extended energy window upto 100 GeV with the full effect of the phases associated with the parameters of LIV in ICAL, (v) combined sensitivity for long-baseline and atmospheric experiments and (vi) detailed comparison of all the available bounds.

The paper is organized as follows. In the next section, we will briefly discuss the theory of LIV and show how it changes the Hamiltonian of the neutrino oscillations. In section 3

¹When our paper was in the final stage of preparation, two papers appeared in the arXiv which study LIV in long-baseline experiments. Ref. [12] study LIV in the context of DUNE and Ref. [13] study LIV in the context of DUNE and T2HK. In our paper, we will not discuss the results of these two papers.

we will discuss the experimental configurations that we use in our analysis. In section 4, we study the effect of LIV at the probability level and in section 5 we present the sensitivity of the experiments in terms of their capability to put upper bound on the LIV parameters. After that in section 6 we compare our results with the results obtained in the previous works. Finally in section 7 we will summarize our results and then conclude.

2 LIV and its effect on neutrino oscillation

Lorentz Invariance violating neutrinos and antineutrinos are effectively described by the Lagrangian density,

$$\mathcal{L} = \frac{1}{2}\bar{\psi}(i\not{\partial} - M - \hat{\mathcal{Q}})\psi + h.c. \quad (2.1)$$

where, $\hat{\mathcal{Q}}$ is generic Lorentz invariance violating operator and fields related to neutrino and antineutrino are introduced by fermionic spinors ψ and $\bar{\psi}$. The first term of the Eq. 2.1 is kinetic term, second term is mass term and third term is Lorentz violating term. Lorentz violation term is small and treated perturbatively. The Lorentz violating Lagrangian is written for renormalizable Dirac coupling as

$$\mathcal{L}_{\text{LIV}} = \frac{-1}{2} \left[a_{\alpha\beta}^{\mu} \bar{\psi} \alpha \gamma_{\mu} \psi_{\beta} + b_{\alpha\beta}^{\mu} \bar{\psi} \alpha \gamma_5 \gamma_{\mu} \psi_{\beta} - i c_{\alpha\beta}^{\mu\nu} \bar{\psi} \alpha \gamma_{\mu} \partial_{\nu} \psi_{\beta} - i d_{\alpha\beta}^{\mu\nu} \bar{\psi} \alpha \gamma_5 \gamma_{\mu} \partial_{\nu} \psi_{\beta} \right] + h.c. \quad (2.2)$$

The observable effect on the left handed neutrinos is controlled by the combinations

$$(a_L)_{\alpha\beta}^{\mu} = (a + b)_{\alpha\beta}^{\mu}, (c_L)_{\alpha\beta}^{\mu\nu} = (c + d)_{\alpha\beta}^{\mu\nu} \quad (2.3)$$

which are constant hermitian matrices in the flavor space that can modify the standard vacuum Hamiltonian. The first combination is CPT-odd LIV term and second combination is CPT-even LIV term. In this work we will focus on the isotropic component of the Lorentz invariance violating terms and we will fix the (μ, ν) indices to zero. To simplify our notation, from now on, we will denote the parameters $(a_L)_{\alpha\beta}^0$ and $(c_L)_{\alpha\beta}^{00}$ as $a_{\alpha\beta}$ and $c_{\alpha\beta}$.

Explicitly, one can write the Lorentz-violating contribution to the full oscillation Hamiltonian as,

$$H = U M U^{\dagger} + V_e + H_{\text{LIV}} \quad (2.4)$$

where U is the PMNS mixing matrix having three mixing angles θ_{12} , θ_{13} , θ_{23} and one CP phase δ_{CP} , M is the neutrino mass matrix given by

$$M = \frac{1}{2E} \begin{pmatrix} 0 & 0 & 0 \\ 0 & \Delta m_{21}^2 & 0 \\ 0 & 0 & \Delta m_{31}^2 \end{pmatrix} \quad (2.5)$$

with $\Delta m_{21}^2 = m_2^2 - m_1^2$ and $\Delta m_{31}^2 = m_3^2 - m_1^2$ where m_1 , m_2 and m_3 are the masses of the active neutrinos, V_e is the electron potential which introduces matter effects expressed as

$$V_e = \pm \sqrt{2} G_F \begin{pmatrix} N_e & 0 & 0 \\ 0 & 0 & 0 \\ 0 & 0 & 0 \end{pmatrix} \quad (2.6)$$

where G_F is the Fermi constant and N_e is the average electron density along the neutrino's path, N_e is calculated using the 26-layer PREM model of the density profile of the Earth and H_{LIV} is given by

$$H_{\text{LIV}} = \begin{pmatrix} a_{ee} & a_{e\mu} & a_{e\tau} \\ a_{e\mu}^* & a_{\mu\mu} & a_{\mu\tau} \\ a_{e\tau}^* & a_{\mu\tau}^* & a_{\tau\tau} \end{pmatrix} - \frac{4}{3}E \begin{pmatrix} c_{ee} & c_{e\mu} & c_{e\tau} \\ c_{e\mu}^* & c_{\mu\mu} & c_{\mu\tau} \\ c_{e\tau}^* & c_{\mu\tau}^* & c_{\tau\tau} \end{pmatrix} \quad (2.7)$$

Note that here, the diagonal parameters are real and the off-diagonal parameters are complex. Therefore for the diagonal parameters, there is no phase associated with them and for the off-diagonal parameters, there is a phase $\phi_{\alpha\beta}^{a/c}$ with $\alpha \neq \beta$ associated with them. For antineutrinos, the a parameters go to $-(a)^*$ and the c parameters go to c^* , which is equivalent to $Re(a) \rightarrow -Re(a)$ and $Im(c) \rightarrow -Im(c)$. Many studies have already been conducted on sidereal LIV parameters, and their associated bounds are listed in [36]. We have taken isotropic LIV parameters in our study.

3 Experimental configuration

In this section we discuss the experimental configurations of T2HK, DUNE and ICAL that we use in our analysis. As these experiments have different combinations of energy, baselines and matter effects, the sensitivity of one experiment can be complimentary to another. We have simulated T2HK and DUNE using GLoBES [20, 21] and for ICAL we use the software from the INO collaboration. In order to implement LIV in GLoBES, we have written an independent probability engine and then included it in GLoBES. We have also used the same probability engine in ICAL.

3.1 ICAL detector at the INO facility

3.1.1 Detector

INO (India-based neutrino observatory) will be facilitated with a 50 kton magnetized iron calorimeter (ICAL) detector to study oscillations of the atmospheric neutrinos. The resistive plate chambers (RPCs) [5] are active detector elements in ICAL, and iron is a target for atmospheric neutrinos. ICAL will be optimized to be sensitive primarily to atmospheric ν_μ and $\bar{\nu}_\mu$. The detector's structure, with horizontal layers of iron interspersed with RPCs, allows it to have nearly complete coverage to the direction of incoming neutrinos, except for those that produce nearly horizontally travelling μ^\pm . As a result, it is sensitive to a wide range of path lengths. ICAL will be sensitive to μ^\pm energy, μ angle, and total hadron energy [22] deposited in CC (NC) interactions of atmospheric ν_μ ($\bar{\nu}_\mu$) with iron target. RPCs with fast response times can distinguish between upward and downward moving μ^\pm . This discrimination separates neutrinos (antineutrinos) with short path lengths from those with longer path lengths. This separation is critical because the probability of neutrino oscillation is strongly dependent on the path length L . ICAL will be magnetized to about 1.5 T in the plane of iron plates, it will be able to distinguish between ν_μ and $\bar{\nu}_\mu$. Our analysis used an energy cutoff of $E_\mu=1$ GeV to 100 GeV. All of these detector properties

were simulated using the CERN GEANT4 [23] package by ICAL collaboration. In our analysis, we will consider a run-time of 10 years.

3.1.2 Flux

When primary cosmic ray protons and nuclei interact in the atmosphere, they produce secondary "atmospheric" cosmic rays that contain all hadrons and their decay products. These secondaries' spectrum peaks in the GeV range, but extends to high energy with a power-law spectrum. Neutrinos were the final component of secondary cosmic radiation because they interact weakly. It contains ν_e , $\bar{\nu}_e$, ν_μ , and $\bar{\nu}_\mu$. The flavor-ratio defined as the flux ratio of different neutrino flavors such as $\frac{\nu_\mu + \bar{\nu}_\mu}{\nu_e + \bar{\nu}_e}$ should be equal to 2, but as the energy of neutrino increases, we can see it differ from 2. Neutrino flux varies with location and also has seasonal variations. All of these characteristics can be found in Ref [24]. We took atmospheric flux generated for Theni site by Honda et al. [24]. The flux is generated for solar maximum and solar minimum with rock on the top of the detector. We took the average of both the flux and used that for our simulation.

3.1.3 Event Generator

The GENIE event generator generates neutrino nucleon interactions using Monte Carlo simulations. It employs various neutrino flux formats such as HAKKM, BGLRS, and FLUKA for atmospheric neutrino flux. Any flux distribution given in the form of a polynomial equation can also be used. It can generate cross-section files for any material or neutrino with an energy range ranging from few MeV to a few hundred GeV. Cross-section files generated and distributed by Fermi collaboration with GENIE MC [25] can also be used. In GENIE, we can specify our detector geometry (written in GEANT4). The ICAL collaboration has made some changes to GENIE in order to use it for ICAL.

3.1.4 Binning Scheme

In our analysis, we consider three variables: muon energy $E_{\mu^\pm}^{obs}$, observed muon direction $\cos(\theta_{\mu^\pm}^{obs})$, and observed hadron energy E_{had}^{obs} . The hadron energy is calculated as $E_{had}^{true} = E_\nu - E_\mu$. At the generator level, we obtain the true muon energy and angle, which differ from the observed quantities due to detector response. To incorporate the neutrino oscillation in the data, we first use the re-weighting algorithm [26], and then we implement the detector response to data. To account for detector efficiency, we employ muon and hadron lookup [27, 28] tables. We use a Gaussian distribution for muon energy and angle for detector resolution. We use the vavilov distribution function for hadron energy in [28]. We bin the data and analyzed it in a specific binning format. The binning scheme is used in this analysis given below in Table-1.

3.1.5 Systematic uncertainties

For ICAL we have considered five sources of systematic uncertainties. They are: (i) 20% error in flux normalization, (ii) cross-section error of 10%, (iii) tilt error of 5%, (iv) zenith angle error of 5% and (v) 5% total systematic error. The systematic errors are the same for neutrino events and antineutrino events.

Observable	Range	Bin width	No. of bins
E_μ^{obs} (GeV) (15 bins)	[1,11]	1	10
	[11,21]	5	2
	[21,25]	4	1
	[25,50]	25	1
	[50,100]	50	1
$\cos(\theta_\mu^{obs})$ (15 bins)	[-1.0,0.0]	0.1	10
	[0.0,1]	0.2	5
E_{had}^{obs} (GeV) (4bins)	[0,2]	1	2
	[2,4]	2	1
	[4,15]	11	1

Table 1: Three observable E_μ , θ_μ and E_{had} are used in the analysis

3.2 DUNE

DUNE (Deep underground neutrino experiment) is a neutrino experiment with multiple purposes. It is also suitable for long baseline studies, atmospheric neutrino studies, and indirect DM detection studies. We use the most recent DUNE configuration files provided by the collaboration to simulate DUNE for long-baseline case [29]. We assume a total run-time of 7 years, with 3.5 years in neutrino mode and the remaining 3.5 years in antineutrino mode, using an on-axis 40 kt liquid argon far detector (FD) housed at the Homestake Mine in South Dakota over a 1300 km baseline. For both the appearance and disappearance channels, we consider neutrino and antineutrino energies ranging from 0 to 20 GeV. The total number of bins used for reconstructed energy is 71, with 64 bins with 0.125 GeV widths in the energy range of 0 to 8 GeV and 7 bins with variable widths beyond 8 GeV. We include the "wrong-sign" components in the beam when calculating events, whether signal or background. We do so for both $\nu_e/\bar{\nu}_e$ and $\nu_\mu/\bar{\nu}_\mu$ candidate events. Flux uncertainty for DUNE is $\sim 8\%$ and dominated by hadron production uncertainties. ND/FD flux uncertainty is $\sim 0.5\%$ in the peak, but rising to $\sim 2\%$ in the falling edge, and dominated by focusing effects.

3.3 T2HK

For T2HK, we use the configuration described in Ref.[30]. We consider two water-Cerenkov detector tanks with fiducial volumes of 187 kt each, located at Kamioka, 295 km from the neutrino source at J-PARC, with a beam power of 1.3 MW and a total exposure of 27×10^{21} protons on target, corresponding to ten years of operation. The total run-time has been divided into 5 years in neutrino mode and 5 years in anti-neutrino mode. We considered overall normalization error of 4.71% (4.13%) for the appearance (disappearance) channel in neutrino mode and 4.47% (4.15%) for the appearance (disappearance) channel in antineutrino mode for systematic errors. Both the signal and the background have the same systematic error. In T2HK, we used 98 equispaced bins in the range of 0.2 - 10 GeV.

4 Discussion at the probability level

In this section, we will study the effect of LIV at the probability levels for all the three experiments. In our analysis, we have considered one parameter at a time and study the sensitivity of each individual parameter. Therefore, in our study, we have six independent CPT conserving parameters and six independent CPT violating parameters. Note that, if we do not consider one parameter at a time and rather consider all the parameter at the same time, then number of independent parameters in each CPT conserving case and CPT violating case would be five. This is because, when one consider all the parameter at the same time, then one can always subtract a matrix proportional to identity without changing the oscillation probabilities. Therefore, leaving only two of the diagonal parameters to be independent. The values of the LIV parameters used in the probability plots are mentioned in the panel titles/legends. The value of the oscillation parameters used in these figures are given in Table 2. For δ_{CP} , we have considered a value of 0° for ICAL and 0° and -90° for T2HK and DUNE. Our choices of δ_{CP} are motivated by the current best-fit value of this parameter as obtained by the currently running experiment T2K [31] and NO ν A [32]. All the figures are given for normal ordering of the neutrino masses i.e., $\Delta m_{31}^2 > 0$.

4.1 ICAL

To show the effect of LIV in ICAL, we calculated the disappearance channel probability ($\nu_\mu \rightarrow \nu_\mu$) with and without LIV and showed the difference between them as oscillograms i.e., in the $\cos\theta - E$ plane. The energy range for our analysis is 1-100 GeV. In Fig. 1 (2) we show the probability oscillogram for $a_{\alpha\beta}$ ($c_{\alpha\beta}$). In both Fig. 1 and Fig. 2, the first and the second row is for the diagonal LIV parameters and the third and the fourth row is for the off-diagonal LIV parameters. The first and third row corresponds to neutrinos, whereas the second and fourth row corresponds to antineutrinos. The value of $\phi_{\alpha\beta}^{a/c}$ for the off-diagonal LIV parameters are zero in these figures. The main features which we observe from these oscillograms are as follows.

For the diagonal CPT violating LIV parameters, we see that effect of LIV is more in $a_{\mu\mu}$ and $a_{\tau\tau}$ as compared to a_{ee} . For a_{ee} , the effect is more in neutrinos as compared to antineutrinos. For neutrinos a_{ee} can be probed in the energy region of 1 GeV to 20 GeV and for antineutrino it can be probed in the energy region below 1 GeV. For $a_{\mu\mu}$ and $a_{\tau\tau}$, the effect of LIV is similar except some difference in the $\cos\theta$ axis. For these two parameters the effect of LIV is more in antineutrinos as compared to the neutrinos. For the off-diagonal CPT violating LIV parameters, we see that the effect of LIV for $a_{e\mu}$ and $a_{e\tau}$ are same except some difference along the $\cos\theta$ axis. For these two parameters, the effect of LIV is more prominent in neutrinos as compared to antineutrinos. Among the three off-diagonal LIV parameters, $a_{\mu\tau}$ is more sensitive to LIV. For this parameter, the effect of LIV is opposite in neutrinos and antineutrinos in a sense that the blue and yellow colors are interchanged in these two panels. Therefore, as far CPT violating LIV parameters are concerned, we expected to have strong bounds on $a_{\mu\mu}$, $a_{\tau\tau}$ and $a_{\mu\tau}$ in ICAL as compared to the other three parameters.

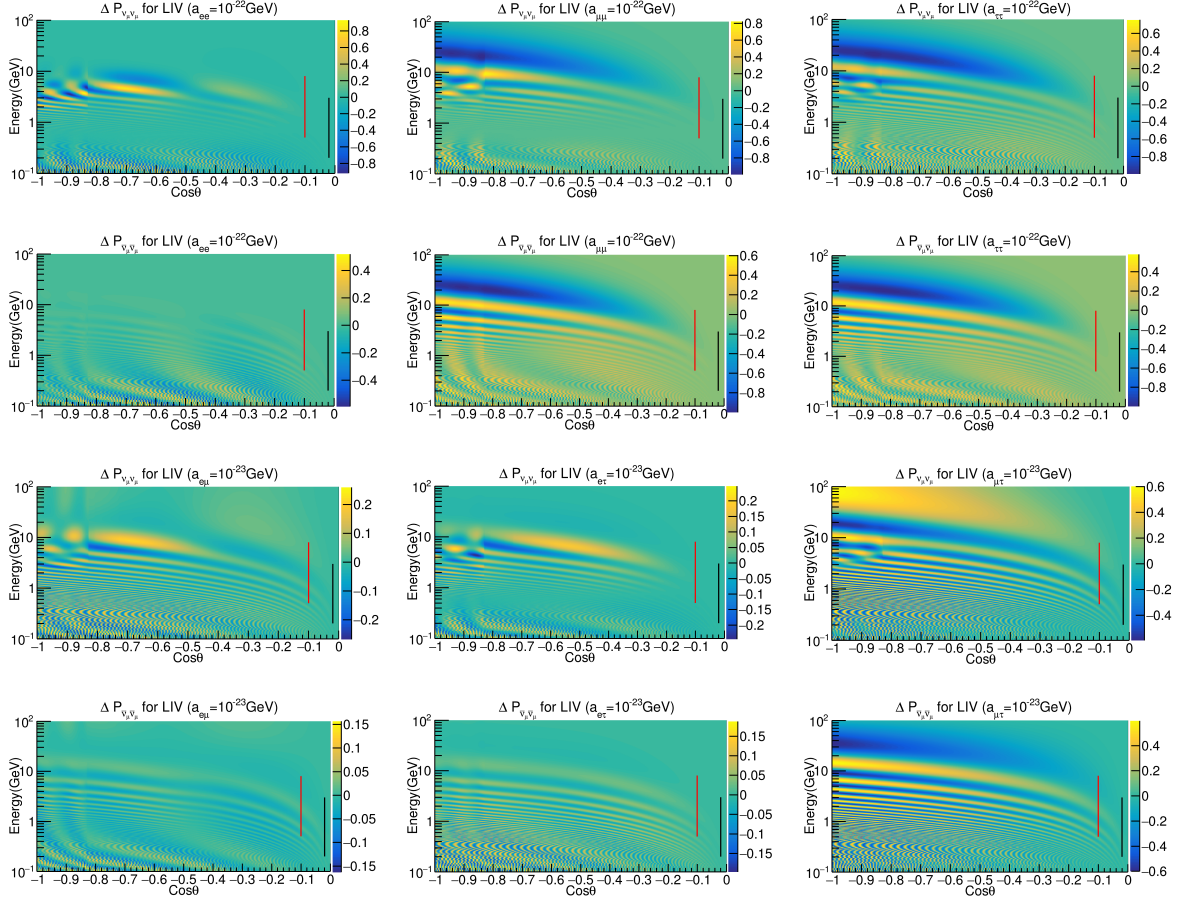


Figure 1: Probability oscillogram for $\Delta P_{\nu_\mu \nu_\mu}$ and $\Delta P_{\bar{\nu}_\mu \bar{\nu}_\mu}$ channels for a_{ee} , $a_{\mu\mu}$, $a_{\tau\tau}$, $a_{e\mu}$, $a_{e\tau}$ and $a_{\mu\tau}$.

Let now discuss the case for CPT conserving parameters. For the diagonal parameters, the behavior of $c_{\alpha\alpha}$ is similar to $a_{\alpha\alpha}$. From the panels we see that the effect of LIV is weak in c_{ee} as compared to other two parameters. For c_{ee} the effect of LIV is in the energy region of 2 GeV to 20 GeV in neutrinos and 0.1 GeV to 10 GeV for antineutrinos. For $c_{\mu\mu}$ and $c_{\tau\tau}$, the effect is similar for neutrinos and antineutrinos except some small difference along the $\cos\theta$ axis. For the off-diagonal parameter $c_{e\mu}$, the effect of LIV is mostly same in neutrinos and antineutrinos. For this parameter, the effect of LIV is visible in 1-10 GeV energy region which has most matter effect for neutrinos but it is absent for antineutrinos. For $c_{e\tau}$, the effect of LIV is more prominent for neutrinos as compared to antineutrinos. The parameter $c_{\mu\tau}$ has similar effect in neutrinos and antineutrinos. From the above discussion we understand that ICAL will have weak bound on c_{ee} as compared to other CPT conserving LIV parameters.

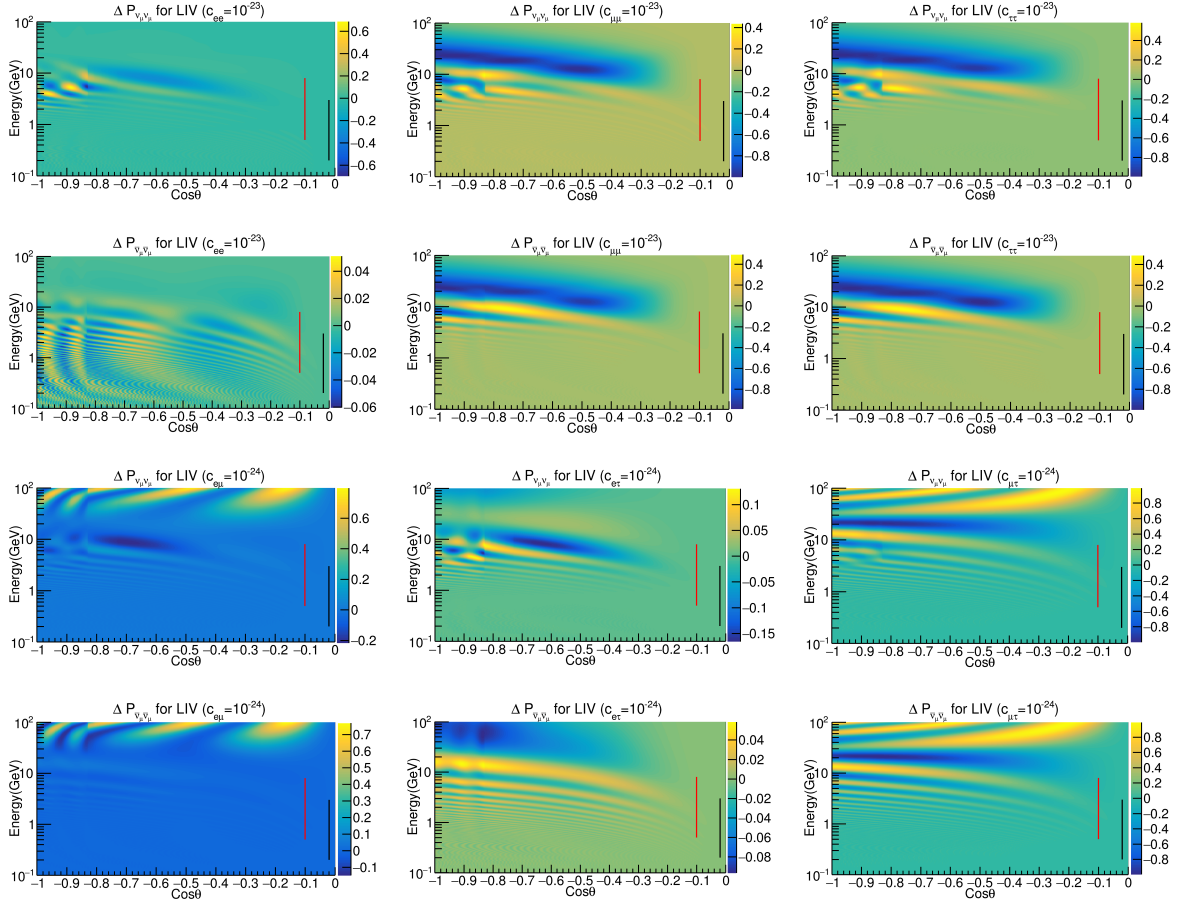


Figure 2: Probability oscillogram for $\Delta P_{\nu_\mu \nu_\mu}$ and $\Delta P_{\bar{\nu}_\mu \bar{\nu}_\mu}$ channels for c_{ee} , $c_{\mu\mu}$, $c_{\tau\tau}$, $c_{e\mu}$, $c_{e\tau}$ and $c_{\mu\tau}$

4.2 DUNE

In figure 3 and figure 4 we have shown the appearance channel ($\nu_\mu \rightarrow \nu_e$) probabilities as a function of E considering DUNE baseline for $a_{\alpha\beta}$ and $c_{\alpha\beta}$ respectively. The first and the second row in both the figures corresponds to diagonal LIV parameters whereas the third and the fourth row corresponds to the off-diagonal LIV parameters. In the first and the third row, the value of δ_{CP} is 0° whereas in the second and the fourth row the value of δ_{CP} is -90° . In each panel the black curve corresponds to the standard oscillations in the three flavor scenario. For the diagonal LIV parameters, we have presented the curves for both positive and negative values of the parameters and for non-diagonal LIV parameters we have presented the curves corresponding to four values of $\phi_{\alpha\beta}^{a/c} = 0^\circ, 90^\circ, 180^\circ$ and 270° . These figures are only for neutrinos. To understand the effect of LIV in the disappearance channel, we refer to Fig. 1 and Fig. 2. The relevant regions in the oscillograms for DUNE are showed by the red line. From these figures, we can deduce the following physics points.

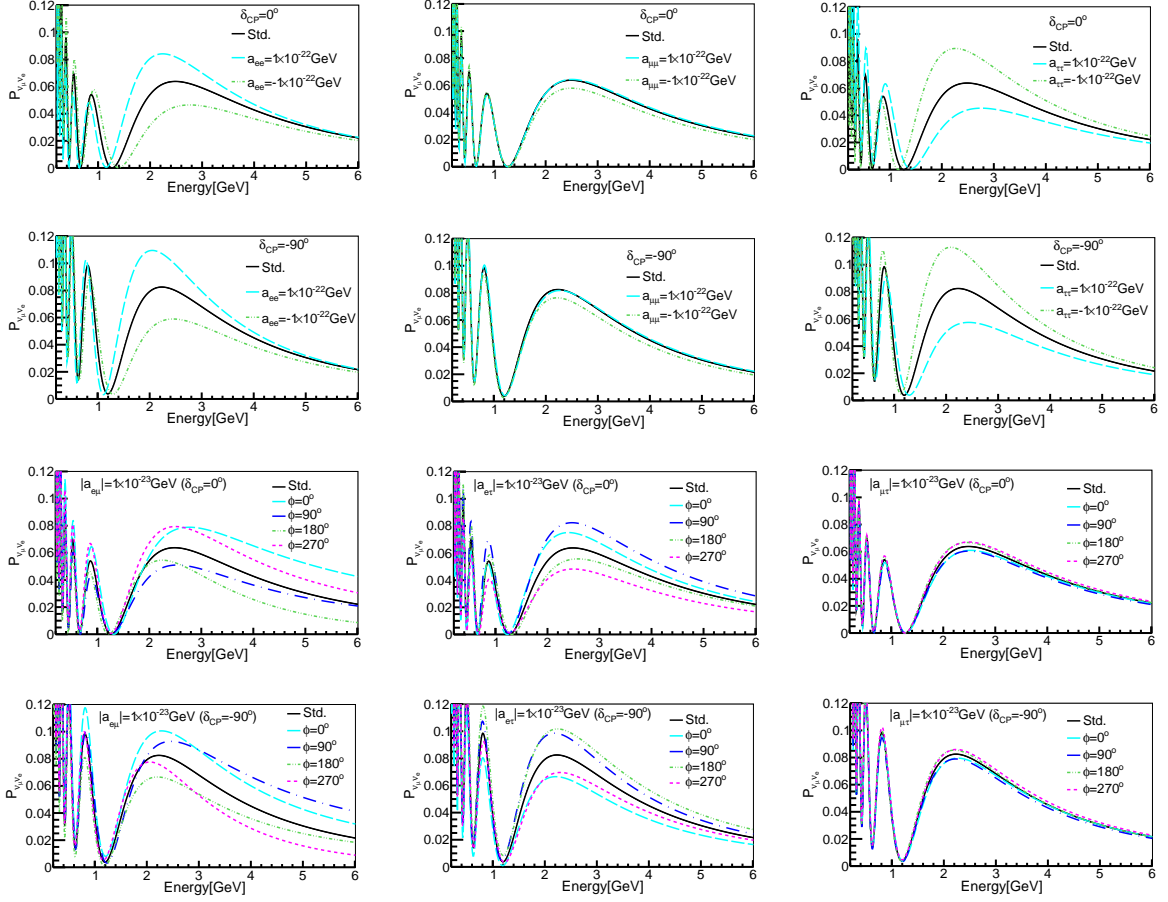


Figure 3: Probability plots for a_{ee} , $a_{\mu\mu}$, $a_{\tau\tau}$ (first/second row is for $\delta_{CP} = 0^\circ / -90^\circ$) and $a_{e\mu}$, $a_{e\tau}$, $a_{\mu\tau}$ (third/fourth row is for $\delta_{CP} = 0^\circ / -90^\circ$) for DUNE setup.

For $a_{\alpha\alpha}$, we see that the parameters a_{ee} and $a_{\tau\tau}$ are more sensitive to LIV as compared to $a_{\mu\mu}$. The effect of LIV for the parameter a_{ee} is opposite to $a_{\tau\tau}$. For a positive value of a_{ee} , the probability is higher as compared to the probability in the standard three flavour scenarios and for a negative value of a_{ee} the probability is lower than the probability in the standard three flavour scenarios. This behavior is opposite for $a_{\tau\tau}$. For $a_{\mu\mu}$ the effect of LIV is negligible. Regarding $a_{\alpha\beta}$ with $\alpha \neq \beta$, the effect of LIV is more in $a_{e\mu}$ and $a_{e\tau}$ as compared to $a_{\mu\tau}$. For a given value of $a_{e\mu}$, the difference with the standard oscillation probability is higher for $\phi_{e\mu}^a = 0^\circ$ and, 180° at $\delta_{CP} = 0^\circ$ and it is higher for $\phi_{e\mu}^a = 90^\circ$ and, 270° at $\delta_{CP} = -90^\circ$. For $a_{e\tau}$, the situation is just opposite to $a_{e\mu}$ i.e., for $\delta_{CP} = 0^\circ$, the separation of the probability with the standard oscillation probability in presence of $a_{e\tau}$ is higher at $\phi_{e\tau}^a = 90^\circ$ and, 270° and for $\delta_{CP} = -90^\circ$, the separation is higher for $\phi_{e\tau}^a = 0^\circ$ and 180° . For DUNE, the effect of LIV on $a_{\mu\tau}$ for the appearance channel is negligible.

In general, CPT conserving parameters are less sensitive to LIV as compared to the CP violating LIV parameters in the appearance channel. For $c_{\alpha\alpha}$, the effect of LIV is similar as that of $a_{\alpha\alpha}$. The parameters c_{ee} and $c_{\tau\tau}$ are more sensitive to LIV as compared to $c_{\mu\mu}$. The effect of LIV for the parameter c_{ee} is opposite to $c_{\tau\tau}$. For a positive value of c_{ee} , the

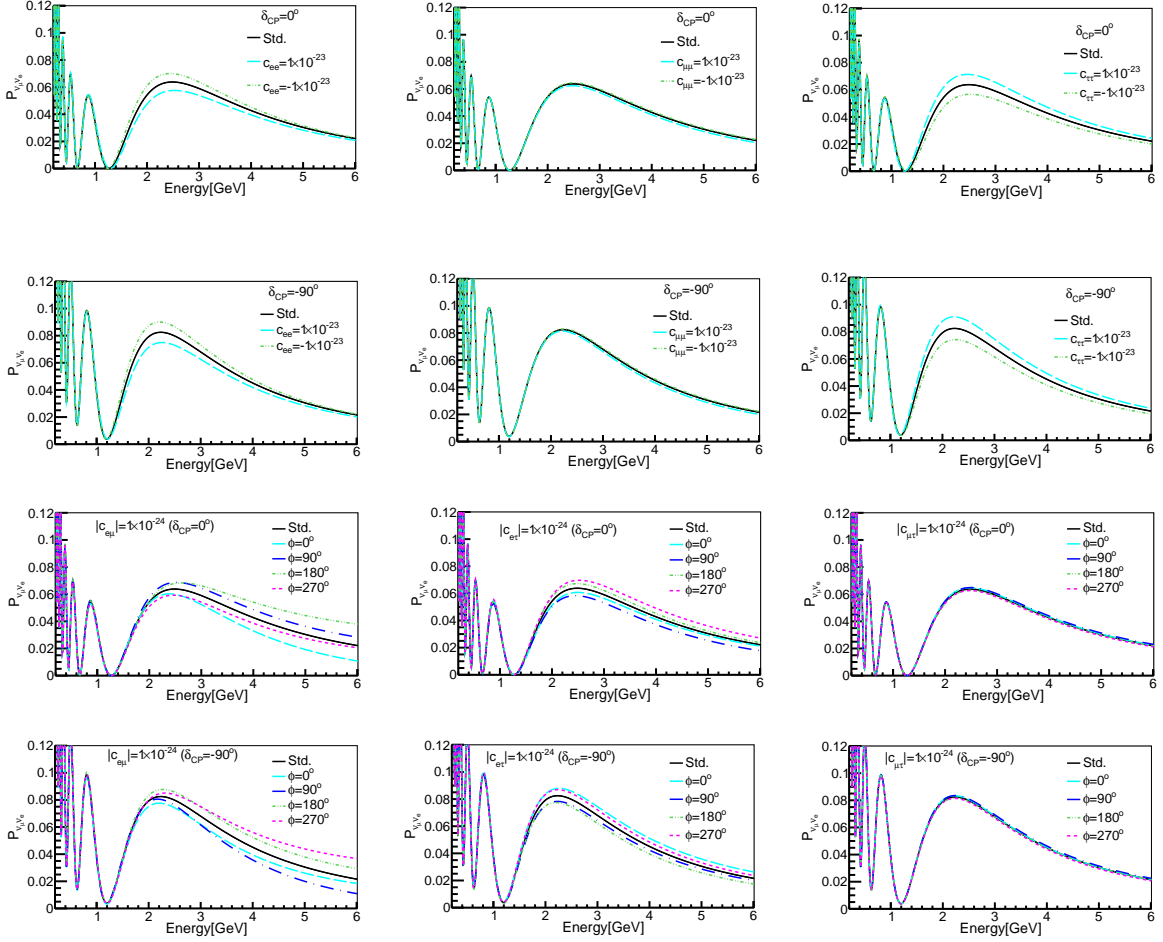


Figure 4: Probability plots for c_{ee} , $c_{\mu\mu}$, $c_{\tau\tau}$ (first/second row is for $\delta_{CP} = 0^\circ / -90^\circ$) and $c_{e\mu}$, $c_{e\tau}$, $c_{\mu\tau}$ ($\delta_{CP} = 0^\circ / -90^\circ$) for DUNE setup.

probability is lower as compared to the probability in the standard three flavour scenarios and for a negative value of c_{ee} the probability is higher than the probability in the standard three flavour scenarios. This behaviour is opposite for $c_{\tau\tau}$. For $c_{\mu\mu}$ the effect of LIV is negligible. Regarding $c_{\alpha\beta}$ with $\alpha \neq \beta$, the behaviour is similar as that of $a_{\alpha\beta}$. The effect of LIV is more in $c_{e\mu}$ and $c_{e\tau}$ as compared to $a_{\mu\tau}$. For a given value of $c_{e\mu}$, the difference with the standard oscillation probability is higher for $\phi_{e\mu}^c = 0^\circ$ and, 180° at $\delta_{CP} = 0^\circ$ and it is higher for $\phi_{e\mu}^c = 90^\circ$ and, 270° at $\delta_{CP} = -90^\circ$. For $c_{e\tau}$, the situation is just opposite to $c_{e\mu}$. The effect of LIV on $c_{\mu\tau}$ is negligible.

Note that, the values of $\phi_{\alpha\beta}$ for which the probability curves are mostly separated from the standard oscillation curve, the strongest bound on this parameter will corresponds to that value of $\phi_{\alpha\beta}$. However, the upper bound on that parameter will corresponds to the value of $\phi_{\alpha\beta}$ for which the sensitivity is worst i.e., for the value of $\phi_{\alpha\beta}$ for which the probability curve is least separated from the standard oscillation curve.

From the above discussion we understand that for DUNE, the appearance channel is

not sensitive to the parameters $a_{\mu\mu}$, $a_{\mu\tau}$, $c_{\mu\mu}$ and $c_{\mu\tau}$. However, some sensitivity to these parameters can come from the disappearance channel. Therefore, when appearance and disappearance channel are combined, it is possible to obtain some finite sensitivity for these four parameters.

4.3 T2HK

In figure 5 we present the same as Fig. 3 but for the T2HK baseline. For disappearance channel, we refer to the black line in Fig. 1. From these panels we see that the behavior of the LIV parameters are exactly same as DUNE but in this case the separation between the probabilities corresponding to LIV and standard three flavour oscillation are very less as compared to DUNE. Therefore, while estimating the bounds, we expect to have same behavior as that of DUNE but significantly less sensitivity as compared to DUNE.

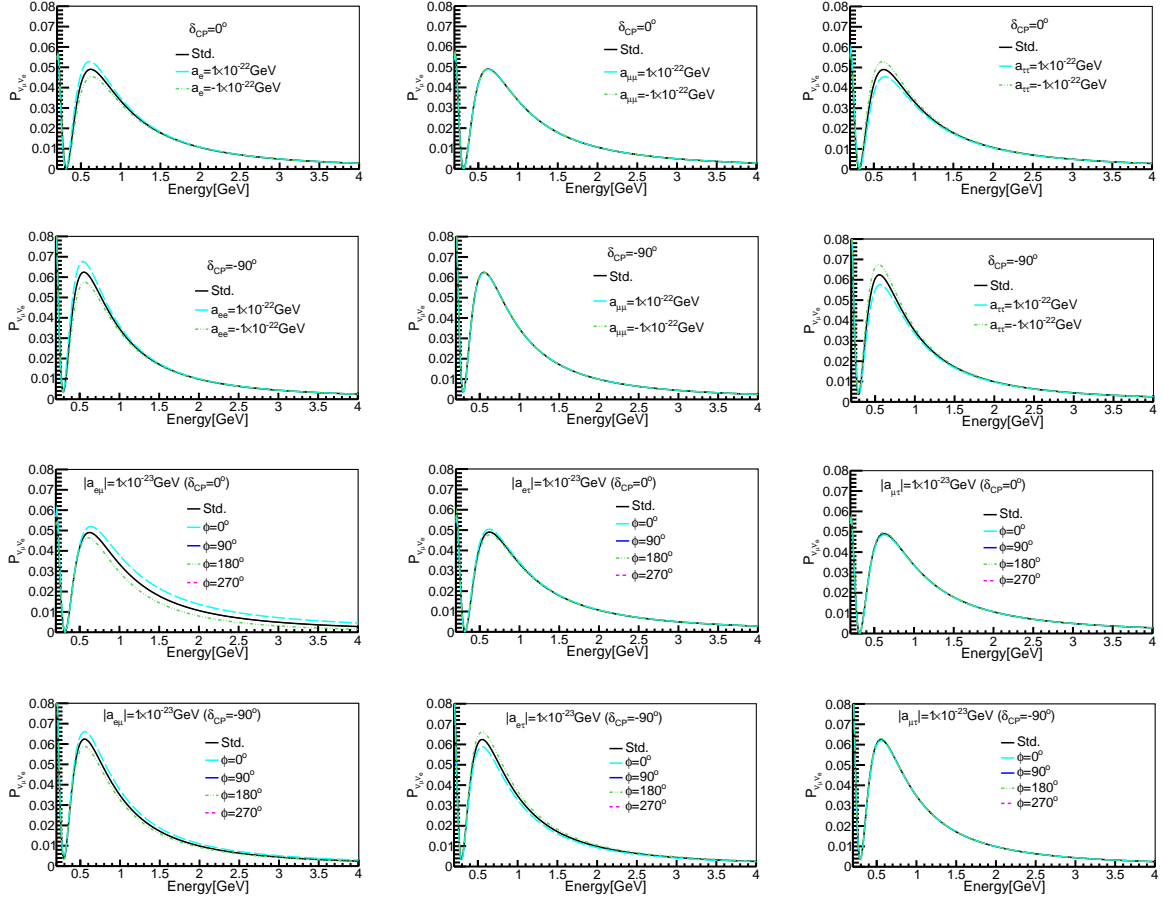


Figure 5: Probability plots for a_{ee} , $a_{\mu\mu}$, $a_{\tau\tau}$ (first/second row is for $\delta_{CP} = 0^\circ / -90^\circ$) and $a_{e\mu}$, $a_{e\tau}$, $a_{\mu\tau}$ (third/fourth row is for $\delta_{CP} = 0^\circ / -90^\circ$) for T2HK setup.

For T2HK, we do not present any figures for CP conserving LIV parameters because we have explicitly checked that for T2HK baseline and energy, the probability curves cor-

responding to standard oscillation and the probability curves for different values of $c_{\alpha\beta}$ are inseparable.

5 Results

In this section we will present the capability of T2HK, DUNE and ICAL to limit the LIV parameters. We will estimate the sensitivity by calculating a χ^2 function defined as [33]:

$$\chi^2 = \sum_i 2 \left[(T_i - D_i) - D_i \ln\left(\frac{T_i}{D_i}\right) \right] + \sum_j \xi_j^2 \quad (5.1)$$

where the sum is over the energy bins for T2HK and DUNE whereas in ICAL the sum is over E_μ , θ_μ and E_{had} bins. The number of events in each bin for theory (data) given by T_i (D_i). To implement the systematic errors, the theory events are varied as:

$$T_i = T_i^0 \left(1 + \sum_j \pi_i^j \xi_j \right) \quad (5.2)$$

where T_i^0 is the corresponding number of events in theory without systematic errors. The pull parameters ξ_j correspond to different sources of systematic uncertainties.

The oscillation parameters that we have used in our calculation are specified in table-2. In our analysis, we used Δm_{eff}^2 in our analysis given by [34, 35]

$$\Delta m_{\text{eff}}^2 = \Delta m_{31}^2 - (\cos^2 \theta_{12} - \cos \delta_{\text{CP}} \sin \theta_{13} \sin 2\theta_{12} \tan \theta_{23}) \Delta m_{21}^2 \quad (5.3)$$

We did marginalization over θ_{23} in range from 40° to 51° , $|\Delta m_{\text{eff}}^2|$ in 3σ range and also the mass ordering. The phases δ_{CP} and $\phi_{\alpha\beta}^{a/c}$ are varied in its full range. For ICAL, we have taken $\delta_{\text{CP}} = 0^\circ$ since χ^2 for ICAL it depends very weakly on δ_{CP} and does not change much for different values of δ_{CP} . For T2HK and DUNE, we have considered two values of δ_{CP} as 0° and -90° . Δm_{21}^2 , θ_{13} and θ_{12} are kept fixed in our analysis. We present our results for the normal ordering of the neutrino masses.

Δm_{21}^2 (eV ²)	Δm_{eff}^2 (eV ²)	$\sin^2 \theta_{12}$	$\sin^2 \theta_{23}$	$\sin^2 2\theta_{13}$	δ_{CP}
7.42×10^{-5}	2.49×10^{-3}	0.33	0.5	0.0875	$0^\circ / -90^\circ$

Table 2: Oscillation parameters used in analysis

5.1 Sensitivity of $a_{\alpha\alpha}$

Let us start our discussion with the diagonal CPT violating LIV parameters. In Fig. 6, we have presented the bounds on the parameters in the χ^2 vs $a_{\alpha\alpha}$ plane. The left column is for $\delta_{\text{CP}} = 0^\circ$ and the right column is for $\delta_{\text{CP}} = -90^\circ$. In each column, different panels corresponds to different $a_{\alpha\alpha}$ parameter. In each panel, we have presented the individual sensitivities of T2HK, DUNE, ICAL and the combined sensitivity of all these three experiments.

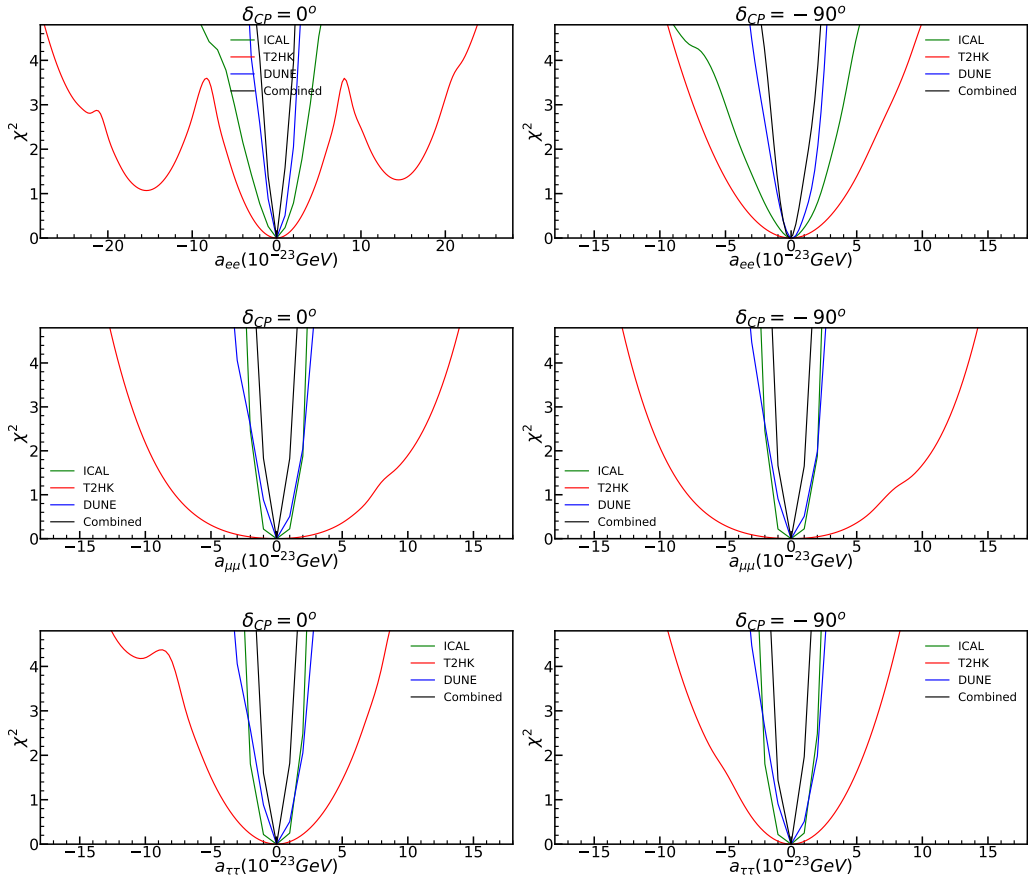


Figure 6: χ^2 as a function of LIV parameters (a_{ee} , $a_{\mu\mu}$ and $a_{\tau\tau}$) for true $\delta_{CP} = 0^\circ$ (left column) and -90° (right column) in ICAL, DUNE, T2HK and combined.

From the discussion on the probability, we understood that regarding a_{ee} , ICAL has weak sensitivity on LIV and for $a_{\mu\mu}$, the sensitivity of DUNE is poor in the appearance channel. For $a_{\tau\tau}$ both DUNE and ICAL are sensitive to LIV. Among all the three experiments, T2HK has the weak dependence of LIV. These features are clearly visible in Fig. 6. From the panels we see that for a_{ee} , DUNE has the best sensitivity. Between $\delta_{CP} = 0^\circ$ and -90° , sensitivity is better for $\delta_{CP} = -90^\circ$. Regarding $a_{\mu\mu}$, ICAL has the best sensitivity. Here we note that though DUNE has a very weak dependence of $a_{\mu\mu}$ on the appearance channel, it has a significant sensitivity with respect to this parameter. This is because in generating the curve for DUNE, we have used both the appearance and disappearance channel and the combination provides a good sensitivity. For $a_{\tau\tau}$, we see that ICAL and DUNE has similar sensitivity for 95% C.L. limit. This can be attributed to the fact that for both ICAL and DUNE are sensitive to this parameter. For $a_{\mu\mu}$ and $a_{\tau\tau}$, the sensitivities corresponding to $\delta_{CP} = 0^\circ$ and -90° are similar. For all the cases, T2HK has the weakest sensitivity. As expected, when we combine the sensitivities of all the three experiments, we obtain the best possible sensitivity for all the parameters. In table 3 we have listed the 95% C.L. sensitivity limit of these parameters for both $\delta_{CP} = 0^\circ$ and -90° .

5.2 Sensitivity of $a_{\alpha\beta}$

Let us now discuss the sensitivities for the non-diagonal CPT violating LIV parameters. In Fig. 7 we present contour plots for at 95% C.L. in the plane $|a_{\alpha\beta}|$ vs $\phi_{\alpha\beta}^a$. The left column is for $\delta_{CP} = 0^\circ$ and the right column is for $\delta_{CP} = -90^\circ$. In each column, different panels corresponds to different $a_{\alpha\beta}$ parameter. In each panel, we have presented the individual sensitivities of T2HK, DUNE, ICAL and the combined sensitivity of all these three experiments.

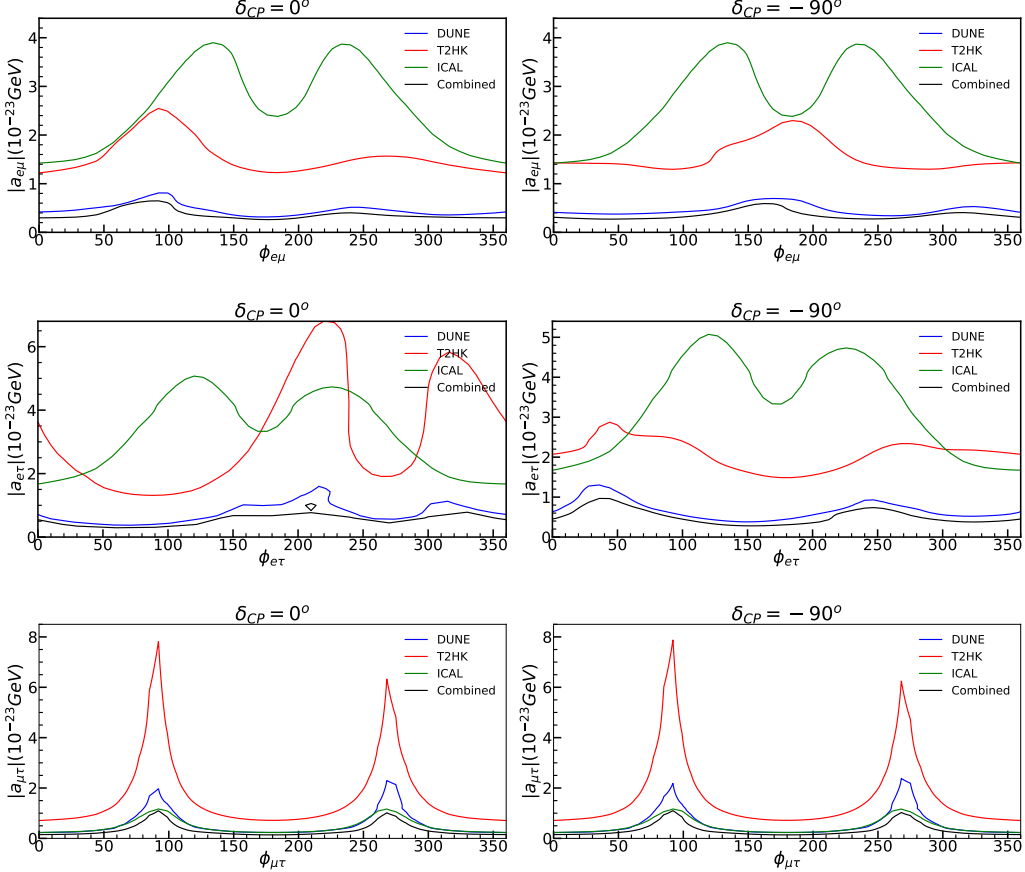


Figure 7: 95% C.L. (2 dof) contour plots between $|a_{\alpha\beta}|$ and LIV parameters $a_{e\mu}$, $a_{e\tau}$ and $a_{\mu\tau}$. Left column is for $\delta_{CP} = 0^\circ$ and right column is for $\delta_{CP} = -90^\circ$.

From the probability level discussion, we have understood that the sensitivity of ICAL is good for $a_{\mu\tau}$ and for long-baseline experiments, we can expect good sensitivity for parameters except $a_{\mu\tau}$. We have also seen that between the two long-baseline experiments, sensitivity of T2HK is weaker than DUNE. Indeed, from Fig. 7, we can observe the expected features. For $a_{e\mu}$, it is interesting to see that the sensitivity of T2HK is weaker than DUNE but it is better than ICAL. In ICAL, the upper bounds for $a_{e\mu}$ and $a_{e\tau}$ correspond to around $\phi_{e\mu}^a/\phi_{e\tau}^a = 120^\circ$ for both values of δ_{CP} . As the long-baseline experiments and ICAL depend on ϕ differently for $a_{e\mu}$ and $a_{e\tau}$, the combination of all the three experiments

may provide a synergy giving the best possible sensitivity. In these two cases, the upper bound corresponds to the same value of ϕ for which the upper bounds of T2HK and DUNE are obtained. For $a_{\mu\tau}$, the best sensitivity comes from ICAL. The sensitivity of T2HK is weaker than DUNE and they both are less sensitive than the sensitivity of ICAL. For this parameter, the upper bound comes at $\phi_{\mu\tau}^a = 90^\circ$ for both values of δ_{CP} and for all the three experiments. Therefore when the three experiments are combined, one gets the upper bound coming at $\phi_{\mu\tau}^a = 90^\circ$. In table 3 we have listed the 95% C.L.(1 dof) sensitivity limit for these parameters at $\delta_{\text{CP}} = 0^\circ$ and -90° .

LIV parameters	ICAL	DUNE	T2HK	Combined
a_{ee}	-6/4.5	-2.84/2.56(-2.7/2.5)	-26/21.6(-8.5/8.8)	-1.95/2.0(-1.9/2.0)
$a_{\mu\mu}$	-2.2/2.2	-2.9/2.5(-2.7/2.4)	-12/13(-12/13.4)	-1.3/1.3(-1.3/1.4)
$a_{\tau\tau}$	-2.3/2.2	-2.9/2.5(-2.7/2.4)	-7.7/8.0(-8.4/7.5)	-1.5/1.5(-1.4/1.4)
$a_{e\mu}$	3.3	0.64(0.56)	2.2(2.0)	0.45(0.4)
$a_{e\tau}$	4.4	1.1(0.9)	5.8(2.3)	0.6(0.63)
$a_{\mu\tau}$	1.0	1.95(2.0)	6.8(6.9)	0.95(0.96)

Table 3: 95% C.L. (1 dof) bounds for ICAL, DUNE, T2HK and their combination in the units of 10^{-23} GeV. For $a_{\alpha\alpha}$, we have given two values. One is corresponding to +ve value and another is for -ve value. For DUNE, T2HK and their combination, we have given two different limits, one is for $\delta_{\text{CP}} = 0^\circ$ (outside parenthesis) and other is for $\delta_{\text{CP}} = -90^\circ$ (inside parenthesis).

5.3 Sensitivity of $c_{\alpha\alpha}$

In this subsection, we will discuss the sensitivity of the different experiments to the diagonal CPT conserving LIV parameters. In Fig. 8, we have plotted the same as Fig. 6 but for $c_{\alpha\alpha}$. In these panels we have not given any curves for T2HK as the sensitivity of T2HK with respect to CPT conserving LIV parameters are very weak.

From the earlier discussion we have seen that ICAL should have good sensitivity to the diagonal CPT conserving LIV parameters except c_{ee} . For long-baseline experiments, we have seen that the behavior of the parameters $c_{\alpha\alpha}$ with respect to the appearance channel probabilities is similar to that of $a_{\alpha\alpha}$, but the changes in the probability due to $c_{\alpha\alpha}$ is somewhat lower than $a_{\alpha\alpha}$. From the panels we see that for c_{ee} , the best sensitivity comes for DUNE and for the other two parameters, the sensitivity of DUNE is poor and the best sensitivity comes from ICAL. When these two experiments are combined, there is an improvement in the sensitivity for c_{ee} but for the other two parameters, addition of DUNE provides only a little improvement in the sensitivity. For all the three parameters, sensitivities are not very different for both values of δ_{CP} . In table 4 we have listed the 95% C.L.(1 dof) sensitivity limit for $\delta_{\text{CP}} = 0^\circ$ and -90° for these parameters.

5.4 Sensitivity of $c_{\alpha\beta}$

In this subsection, we will discuss the sensitivity for the off-diagonal CPT conserving LIV parameters. In Fig. 9, we have given the same as Fig. 7 but for $c_{\alpha\beta}$ (when $\alpha \neq \beta$) without

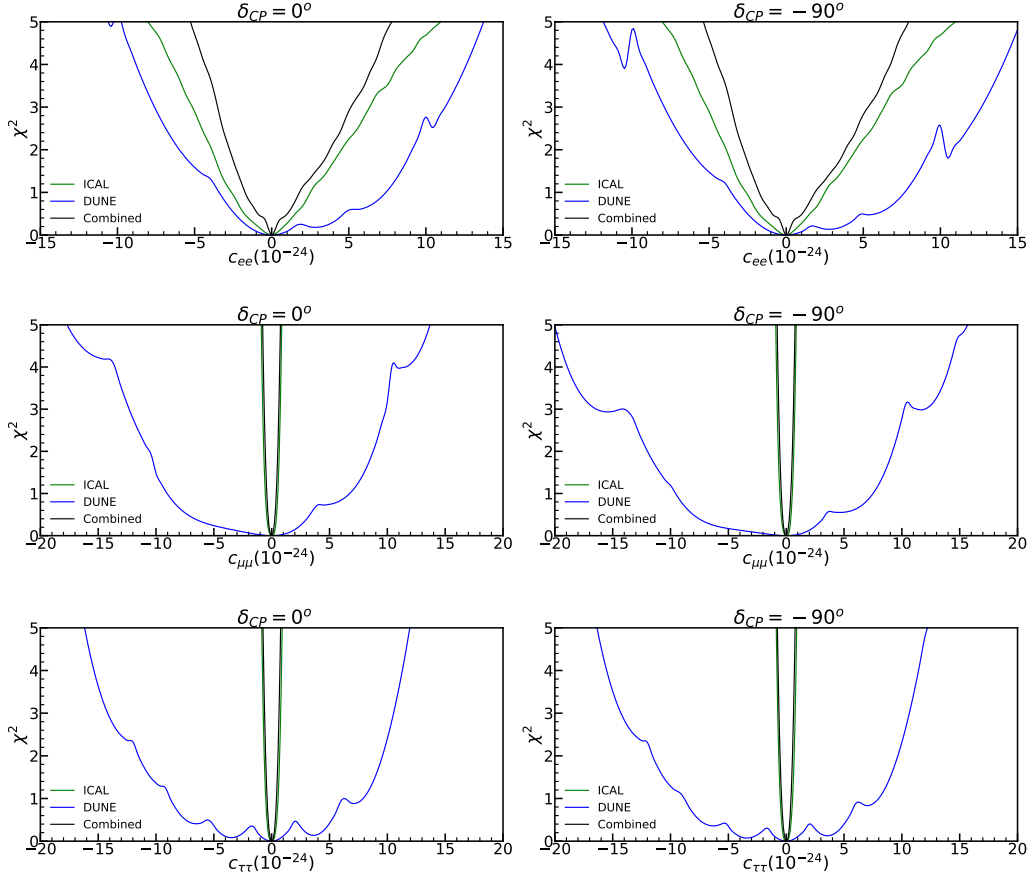


Figure 8: χ^2 as a function of LIV parameters c_{ee} , $c_{\mu\mu}$ and $c_{\tau\tau}$ for true $\delta_{CP} = 0^\circ$ (left column) and -90° (right column) in ICAL, DUNE and combined.

the curves for T2HK.

For these set of parameters, we should get sizable amount of sensitivity from ICAL. Regarding the long-baseline experiments, as understood from the probabilities, the behavior of $c_{\alpha\beta}$ is similar as that of $a_{\alpha\beta}$ with a lower sensitivity. For $c_{e\mu}$, DUNE gives better sensitivity than ICAL except $\delta_{CP} = -90^\circ$ and $\phi_{e\mu}^c = 180^\circ$. For $c_{e\tau}$, the sensitivity of DUNE is better than ICAL in some of the regions depending on the values of δ_{CP} and $\phi_{e\tau}^c$. For DUNE, the upper bound corresponds to $\phi_{e\mu}^c = 50^\circ$ for $\delta_{CP} = 0^\circ$ and $\phi_{e\mu}^c = 90^\circ$ for $\delta_{CP} = -90^\circ$ in $c_{e\mu}$. For $c_{e\tau}$, the upper bound comes at $\phi_{e\tau}^c = 10^\circ$ for $\delta_{CP} = 0^\circ$ and $\phi_{e\tau}^c = 90^\circ$ for $\delta_{CP} = -90^\circ$ in DUNE. For ICAL, the upper bound comes at $\phi^c = 90^\circ$ for both $c_{e\mu}$ and $c_{e\tau}$. For these two parameters, the sensitivity improves when DUNE and ICAL are combined and in this case the upper bound corresponds to around $\phi_{e\mu}^c = 90^\circ$. For $c_{\mu\tau}$, the sensitivity of DUNE is weak as compared to ICAL. Therefore when combined the improvement in the sensitivity is very marginal. In this case the upper bound corresponds to $\phi_{\mu\tau}^c = 90^\circ$. For this parameter, the sensitivity is similar for both the values of δ_{CP} . In table 4 we have listed the 95% C.L.(1 dof) sensitivity limit of these parameters for both values of δ_{CP} .

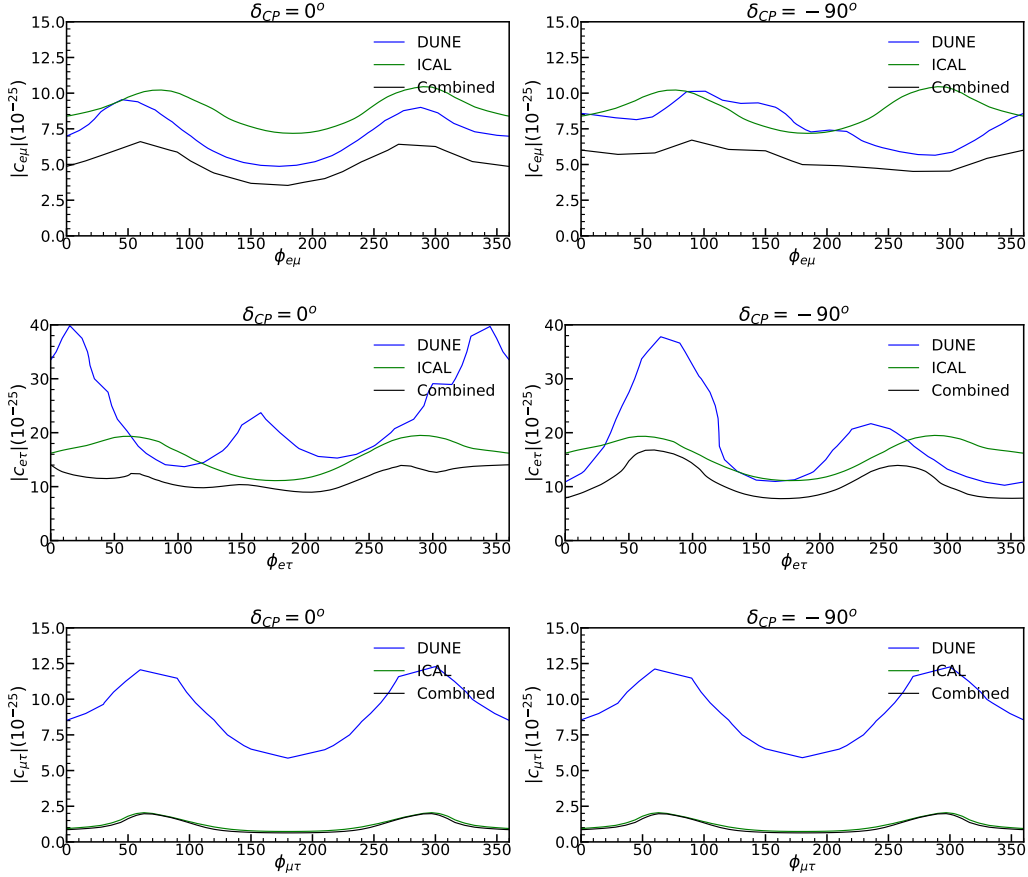


Figure 9: 95% C.L. (2 dof) contour plots between $|c_{\alpha\beta}|$ and LIV parameters $c_{e\mu}$, $c_{e\tau}$ and $c_{\mu\tau}$. Left column is for $\delta_{CP} = 0^\circ$ and right column is for $\delta_{CP} = -90^\circ$.

LIV parameters	ICAL	DUNE	Combined
c_{ee}	-62/80	-86/124(-90/140)	-41/80(-43/65)
$c_{\mu\mu}$	-9.4/7.3	-136/103(187/140)	-7.8/6(-7.5/7.6)
$c_{\tau\tau}$	-8/8.5	-155/112(-153/113)	-6.1/6.5(-6.9/6.3)
$c_{e\mu}$	7.8	8.2(8.9)	5.5(5.2)
$c_{e\tau}$	16.8	34(32.02)	11(13.8)
$c_{\mu\tau}$	1.6	11.0(11.0)	1.6(1.6)

Table 4: 95% C.L.(1 dof) bounds for ICAL, DUNE and their combination in the units of 10^{-25} . For $c_{\alpha\alpha}$ parameters, we have given two values. One is corresponding to +ve value and another is for -ve value. For DUNE, T2HK and their combination, we have given two different limits, one is for $\delta_{CP} = 0^\circ$ (outside parenthesis) and other is for $\delta_{CP} = -90^\circ$ (inside parenthesis).

6 Comparison with previous results

In this section, we provide the comparison of the results that we obtain in this present work with the previous results. Note that in our study, the LIV parameters that we consider are model independent. Bounds on the LIV parameters coming from different standard model extensions are listed in Ref. [36]. In table 5, we have compiled, all the existing bounds on the LIV parameters along with our bounds for the combined ICAL, T2HK and DUNE. For $a_{\alpha\beta}$, we present the bounds for ICAL+T2HK+DUNE and for $c_{\alpha\beta}$, we present the bounds for ICAL+DUNE. For individual bounds coming from these experiments, we refer to tables 3 and 4. Further, in figure 10, we have presented a bar chart, showing the comparison between our bounds as obtained in the combined DUNE+T2HK+ICAL (for $a_{\alpha\beta}$) or ICAL+DUNE (for $c_{\alpha\beta}$) and the current best available bounds on the LIV parameters.

Note that study of LIV parameters in the context of DUNE and ICAL has been studied earlier. First, we would like to point out the features which are new in our analysis.

- Ref. [11] studied CPT odd LIV parameters for off diagonal elements ($a_{\alpha\beta}$, for $\alpha \neq \beta$) for ICAL. They have assumed that complex phases have very small effect on sensitivity results. In their analysis, they used nuance MC generator for event generation. Further, they used muon energy range of 1 to 25 GeV. In our analysis we have considered the effect of $\phi_{\alpha\beta}$ which have nontrivial effect on the LIV parameters. We used GENIE MC for event generation, which uses updated cross-section values. We also used an extended binning scheme where we extended muon energy range from 25 GeV to 100 GeV. Due to this our results are stronger as compared to the results obtained in Ref. [11].
- Ref [6] study CPT odd LIV parameters in DUNE and in Ref. [10], they have combined P2O with DUNE. In these references, they used the conceptual design report of DUNE (CDR) [37] for detector configuration, efficiency, resolution and systematic uncertainties. In our analysis we used recent published technical design report of DUNE (TDR) [38] to build our detector setup and used new efficiency, resolution and systematic uncertainties. These changes improved our sensitivity as compared to Ref. [6].

Now let us compare the bounds for the individual parameters as obtained from different experiments.

- The CPT odd diagonal parameters $a_{\alpha\alpha}$ are studied in the context of DUNE [6], T2K+NO ν A [17] and DUNE+P2O [10]. In Refs. [10] and [6], they have considered only two independent diagonal parameters as $a_{ee} - a_{\tau\tau}$ and $a_{\mu\mu} - a_{\tau\tau}$. In Ref. [17], they have taken all three as independent parameters as a_{ee} , $a_{\mu\mu}$ and $a_{\tau\tau}$. In our work, we have also taken all three diagonal parameters as independent parameters. From table 5 we see that our results give the best sensitivity for a_{ee} .
- The CPT odd off-diagonal parameters $a_{\alpha\beta}$ (for $\alpha \neq \beta$) are studied in all the experiments that are listed in table 5. For all the parameter $a_{e\mu}$, the combination of ICAL, T2HK and DUNE provides the best sensitivity.

- We have studied $c_{\alpha\alpha}$ in atmospheric neutrinos in ICAL detector setup and also in long baseline experiment DUNE. The parameter $c_{\tau\tau}$ is studied in IceCube [15] and the bound obtained is stronger than our results². The other two CPT even diagonal parameters c_{ee} and $c_{\mu\mu}$ are not studied in any literature. Our work provides the first ever bounds on these parameters.
- The CPT even off-diagonal parameters $c_{\alpha\beta}$ (for $\alpha \neq \beta$) are studied in the context of SK [14] and IceCube [15]. In our work, we have simulated results for DUNE and ICAL detector setups. Our results are comparable to SK for $c_{e\tau}$ only. For $c_{e\mu}$ SK has given the best limit and for $c_{\mu\tau}$ IceCube has given the strongest limit.

Experiments	Details	95% C.L.(1 dof) $a_{\alpha\beta}$ in GeV ($c_{\alpha\beta}$)	Ref.
SK (Atmospheric)	SK atmospheric data	$e\mu = 1.8 \times 10^{-23}$ (8×10^{-27}) $e\tau = 2.8 \times 10^{-23}$ (9.3×10^{-25}) $\mu\tau = 5.1 \times 10^{-24}$ (4.4×10^{-27})	[14]
IceCube	IceCube data analyzed for $\mu\tau$ LIV parameters for 3, 4, 5, 6 and 7 dim. operators	$\mu\tau = 2.0 \times 10^{-24}$ (2.7×10^{-28}) 90% C.L. $\tau\tau = 2.0 \times 10^{-26}$ (2.0×10^{-31}) 90% C.L.	[15]
ICAL	Atmospheric neutrino simulated between 1-25 GeV range for $a_{\alpha\beta}$	$e\mu = 1.34 \times 10^{-23}$ (N.A.) $e\tau = 1.58 \times 10^{-23}$ (N.A.) $\mu\tau = 2.2 \times 10^{-24}$ (N.A.)	[11]
DUNE	Long-baseline neutrino simulated between 0.2-10 GeV range for $a_{\alpha\alpha}$ and $a_{\alpha\beta}$	$e\mu = 7 \times 10^{-24}$ (N.A.) $e\tau = 1.0 \times 10^{-23}$ (N.A.) $\mu\tau = 1.7 \times 10^{-23}$ (N.A.) $ee = (-2.5, 3.2) \times 10^{-23}$ (N.A.) $\mu\mu = (-3.7, 2.8) \times 10^{-23}$ (N.A.)	[6]
T2K+NOVA	NOVA and T2K long-baseline experiments simulation for LIV sensitivity for $a_{\alpha\alpha}$ and $a_{\alpha\beta}$	$e\mu = 3.6 \times 10^{-23}$ (N.A.) $e\tau = 1.08 \times 10^{-22}$ (N.A.) $\mu\tau = 8 \times 10^{-23}$ (N.A.) $ee = (-5.5, 3.4) \times 10^{-22}$ (N.A.) $\mu\mu = (-1.07, 1.18) \times 10^{-22}$ (N.A.) $\tau\tau = (-1.12, 0.9) \times 10^{-22}$ (N.A.)	[17]
DUNE+P2O	Long-baseline DUNE and P2O data simulated for LIV sensitivity for $a_{\alpha\alpha}$ and $a_{\alpha\beta}$	$e\mu = 4.7 \times 10^{-24}$ (N.A.) $e\tau = 6 \times 10^{-24}$ (N.A.) $\mu\tau = 1.3 \times 10^{-23}$ (N.A.) $ee = (-2.6, 3.3) \times 10^{-23}$ (N.A.) $\mu\mu = (-1.5, 1.6) \times 10^{-23}$ (N.A.)	[10]
ICAL+T2HK+DUNE ($a_{\alpha\beta}$) ICAL+DUNE ($c_{\alpha\beta}$)	Combining atmospheric and long-baseline experiments with $a_{\alpha\alpha}$, $a_{\alpha\beta}$, $c_{\alpha\alpha}$ and $c_{\alpha\beta}$. ICAL with extended range 1-100 GeV. DUNE with recent TDR included. Exploring $\phi_{\alpha\beta}$ impact on experiments and combined analysis.	$e\mu = 4 \times 10^{-24}$ (5.1×10^{-25}) $e\tau = 6 \times 10^{-24}$ (1.1×10^{-24}) $\mu\tau = 9.5 \times 10^{-24}$ (1.6×10^{-25}) $ee = (-2.1, 2.1) \times 10^{-23}$ ($(-4.2, 6.5) \times 10^{-24}$) $\mu\mu = (-1.8, 1.9) \times 10^{-23}$ ($(-7.4, 6) \times 10^{-25}$) $\tau\tau = (-1.5, 1.5) \times 10^{-23}$ ($(-6.7, 6.4) \times 10^{-25}$)	This work

Table 5: 95% C.L. (1 dof) limit of the LIV parameters from available literature, except for IceCube. For IceCube, the bounds are available only at 90% C.L.

²Note that the bound for IceCube which is listed in table 5 is given at 90% C.L., whereas our results are given at 95% C.L.

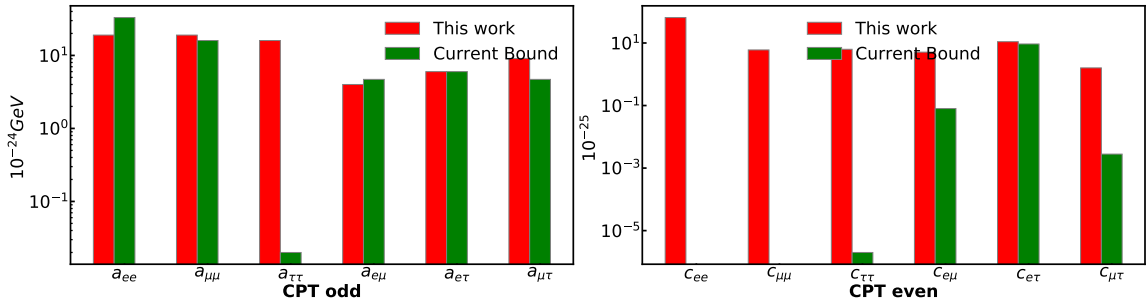


Figure 10: In the left panel, we have shown our limit for CPT odd parameters (red bars) and current best bounds (green bars) which are listed in table 5. In right panel, we have shown results for CPT even parameters. Note that the current bound for $c_{\tau\tau}$ is at 90% C.L. whereas all the other bounds are at 95% C.L.

7 Summary and conclusion

In this paper, we have presented a comprehensive study of Lorentz Invariance Violation (LIV) in the context of atmospheric neutrino experiment ICAL and long-baseline experiments T2HK and DUNE. In our study we consider the full parameter space of the LIV parameters, i.e., six CPT violating LIV parameters ($a_{\alpha\beta}$) and six CPT conserving LIV parameters ($c_{\alpha\beta}$). In this study, our objective is to calculate the upper bound on all the LIV parameters with respect to the individual experiments and their combination. Note that some of LIV parameters are studied in the context of ICAL and DUNE. However, the specifications of these experiments used in the present study are different as compared to the previous studies. For DUNE, we have used the configuration from the latest technical design report, whereas for ICAL, we have used an extended energy region of 1 GeV to 100 GeV. Further, in ICAL we have studied the effect of the phases associated with the LIV parameters, which was not the case for the earlier study of LIV with ICAL. Due to this, our results are improved as compared to previous results.

For ICAL, the sensitivity to LIV parameters mainly comes from the disappearance channel whereas for DUNE and T2HK, the sensitivity can come from both appearance and disappearance channel. At the probability level we have shown that ICAL is mainly sensitive to $a_{\mu\mu}$, $a_{\tau\tau}$ and $a_{\mu\tau}$ as far as the CPT violating LIV parameters are concerned. For the CPT conserving LIV parameters, ICAL is sensitive to all the parameters except c_{ee} . For DUNE, we have shown that the appearance channel is not sensitive to the parameters $a_{\mu\mu}$, $a_{\mu\tau}$, $c_{\mu\mu}$ and $c_{\mu\tau}$. For T2HK, it is sensitive to the same parameters as DUNE as far as the CPT violating LIV parameters are concerned. However, in this the sensitivity is weak as compared to DUNE. We have also found that T2HK is not sensitive to the CPT conserving LIV parameters. At the χ^2 level, we find that the results are consistent with the conclusions that we derived from the oscillation probabilities. Among the three experiments, DUNE gives the best sensitivity on a_{ee} , $a_{e\mu}$, $a_{e\tau}$ and $a_{\mu\tau}$ whereas ICAL gives the best sensitivity on $a_{\mu\mu}$, c_{ee} , $c_{\mu\mu}$, $c_{\tau\tau}$, $c_{e\mu}$, $c_{e\tau}$ and $c_{\mu\tau}$. For $a_{\tau\tau}$, the sensitivity of DUNE and ICAL are similar. While comparing with the existing bounds on the LIV parameters

from different experiments with the one obtained with the combination of T2HK, DUNE and ICAL (i.e., bounds from ICAL+T2HK+DUNE on $a_{\alpha\beta}$ and bounds from ICAL+DUNE on $c_{\alpha\beta}$), we find that for the parameters a_{ee} ($a_{\mu\mu}$) our results are better (comparable) with DUNE+P2O. For the parameter $a_{e\mu}$, the strongest bounds are from our results. For $c_{e\mu}$ SK has given best limit and $c_{\mu\tau}$ IceCube has given the strongest limit. The bounds from SK on $c_{e\tau}$ is similar to what we obtained from the combination of DUNE and ICAL. For the diagonal CPT conserving LIV parameters, our work provides the first ever bounds on c_{ee} and $c_{\mu\mu}$.

Acknowledgments

This work is performed by the members of the INO-ICAL collaboration. We thank the members of the INO-ICAL collaboration for their valuable comments and constructive inputs. The HRI cluster computing facility (<http://cluster.hri.res.in>) is gratefully acknowledged.

References

- [1] V. A. Kostelecky and S. Samuel, *Spontaneous Breaking of Lorentz Symmetry in String Theory*, *Phys. Rev. D* **39** (1989) 683.
- [2] D. Colladay and V. A. Kostelecky, *Lorentz violating extension of the standard model*, *Phys. Rev. D* **58** (1998) 116002, [[hep-ph/9809521](https://arxiv.org/abs/hep-ph/9809521)].
- [3] **Hyper-Kamiokande** Collaboration, K. Abe et al., *Physics potentials with the second Hyper-Kamiokande detector in Korea*, *PTEP* **2018** (2018), no. 6 063C01, [[arXiv:1611.06118](https://arxiv.org/abs/1611.06118)].
- [4] **DUNE** Collaboration, B. Abi et al., *Deep Underground Neutrino Experiment (DUNE), Far Detector Technical Design Report, Volume II: DUNE Physics*, [arXiv:2002.03005](https://arxiv.org/abs/2002.03005).
- [5] **ICAL** Collaboration, S. Ahmed et al., *Physics Potential of the ICAL detector at the India-based Neutrino Observatory (INO)*, *Pramana* **88** (2017), no. 5 79, [[arXiv:1505.07380](https://arxiv.org/abs/1505.07380)].
- [6] G. Barenboim, M. Masud, C. A. Ternes, and M. Tórtola, *Exploring the intrinsic Lorentz-violating parameters at DUNE*, *Phys. Lett. B* **788** (2019) 308–315, [[arXiv:1805.11094](https://arxiv.org/abs/1805.11094)].
- [7] S. Kumar Agarwalla and M. Masud, *Can Lorentz invariance violation affect the sensitivity of deep underground neutrino experiment?*, *Eur. Phys. J. C* **80** (2020), no. 8 716, [[arXiv:1912.13306](https://arxiv.org/abs/1912.13306)].
- [8] **KM3Net** Collaboration, S. Adrian-Martinez et al., *Letter of intent for KM3NeT 2.0*, *J. Phys. G* **43** (2016), no. 8 084001, [[arXiv:1601.07459](https://arxiv.org/abs/1601.07459)].
- [9] A. V. Akindinov et al., *Letter of Interest for a Neutrino Beam from Protvino to KM3NeT/ORCA*, *Eur. Phys. J. C* **79** (2019), no. 9 758, [[arXiv:1902.06083](https://arxiv.org/abs/1902.06083)].
- [10] N. Fiza, N. R. Khan Chowdhury, and M. Masud, *Investigating Lorentz Violation with the long baseline experiment P2O*, [arXiv:2206.14018](https://arxiv.org/abs/2206.14018).
- [11] S. Sahoo, A. Kumar, and S. K. Agarwalla, *Probing Lorentz Invariance Violation with atmospheric neutrinos at INO-ICAL*, *JHEP* **03** (2022) 050, [[arXiv:2110.13207](https://arxiv.org/abs/2110.13207)].

- [12] A. Sarker, A. Medhi, and M. M. Devi, *Investigating the effects of Lorentz Invariance Violation on the CP-sensitivities of the Deep Underground Neutrino Experiment*, [arXiv:2302.10456](#).
- [13] S. K. Agarwalla, S. Das, S. Sahoo, and P. Swain, *Constraining Lorentz Invariance Violation with Next-Generation Long-Baseline Experiments*, [arXiv:2302.12005](#).
- [14] **Super-Kamiokande** Collaboration, K. Abe et al., *Test of Lorentz invariance with atmospheric neutrinos*, *Phys. Rev. D* **91** (2015), no. 5 052003, [[arXiv:1410.4267](#)].
- [15] **IceCube** Collaboration, M. G. Aartsen et al., *Neutrino Interferometry for High-Precision Tests of Lorentz Symmetry with IceCube*, *Nature Phys.* **14** (2018), no. 9 961–966, [[arXiv:1709.03434](#)].
- [16] A. Crivellin, F. Kirk, and M. Schreck, *Implications of $SU(2)_L$ gauge invariance for constraints on Lorentz violation*, *JHEP* **04** (2021) 082, [[arXiv:2009.01247](#)].
- [17] R. Majhi, S. Chembra, and R. Mohanta, *Exploring the effect of Lorentz invariance violation with the currently running long-baseline experiments*, *Eur. Phys. J. C* **80** (2020), no. 5 364, [[arXiv:1907.09145](#)].
- [18] H.-X. Lin, J. Tang, S. Vihonen, and P. Pasquini, *Nonminimal Lorentz invariance violation in light of the muon anomalous magnetic moment and long-baseline neutrino oscillation data*, *Phys. Rev. D* **105** (2022), no. 9 096029, [[arXiv:2111.14336](#)].
- [19] U. Rahaman, *Looking for Lorentz invariance violation (LIV) in the latest long baseline accelerator neutrino oscillation data*, *Eur. Phys. J. C* **81** (2021), no. 9 792, [[arXiv:2103.04576](#)].
- [20] P. Huber, M. Lindner, and W. Winter, *Simulation of long-baseline neutrino oscillation experiments with GLOBES (General Long Baseline Experiment Simulator)*, *Comput. Phys. Commun.* **167** (2005) 195, [[hep-ph/0407333](#)].
- [21] P. Huber, J. Kopp, M. Lindner, M. Rolinec, and W. Winter, *New features in the simulation of neutrino oscillation experiments with GLOBES 3.0: General Long Baseline Experiment Simulator*, *Comput. Phys. Commun.* **177** (2007) 432–438, [[hep-ph/0701187](#)].
- [22] S. M. Lakshmi, A. Ghosh, M. M. Devi, D. Kaur, S. Choubey, A. Dighe, D. Indumathi, M. V. N. Murthy, and M. Naimuddin, *Simulation studies of hadron energy resolution as a function of iron plate thickness at INO-ICAL*, *Journal of Instrumentation* **9** (sep, 2014) T09003–T09003.
- [23] S. Agostinelli, J. Allison, and G. collaboration, *Geant4—a simulation toolkit*, *Nuclear Instruments and Methods in Physics Research Section A: Accelerators, Spectrometers, Detectors and Associated Equipment* **506** (2003), no. 3 250–303.
- [24] M. Honda, M. S. Athar, T. Kajita, K. Kasahara, and S. Midorikawa, *Atmospheric neutrino flux calculation using the nrlmsise-00 atmospheric model*, *Phys. Rev. D* **92** (Jul, 2015) 023004.
- [25] C. Andreopoulos et al., *The GENIE Neutrino Monte Carlo Generator*, *Nucl. Instrum. Meth. A* **614** (2010) 87–104, [[arXiv:0905.2517](#)].
- [26] V. Barger, K. Whisnant, S. Pakvasa, and R. J. N. Phillips, *Matter effects on three-neutrino oscillations*, *Phys. Rev. D* **22** (Dec, 1980) 2718–2726.
- [27] A. Chatterjee, K. K. Meghna, R. Kanishka, T. Thakore, V. Bhatnagar, R. Gandhi, D. Indumathi, N. K. Mondal, and N. Sinha, *A simulations study of the muon response of the*

- iron calorimeter detector at the india-based neutrino observatory*, *Journal of Instrumentation* **9** (jul, 2014) P07001–P07001.
- [28] M. M. Devi, A. Ghosh, D. Kaur, L. S. Mohan, S. Choubey, A. Dighe, D. Indumathi, S. Kumar, M. V. N. Murthy, and M. Naimuddin, *Hadron energy response of the Iron Calorimeter detector at the India-based Neutrino Observatory*, *JINST* **8** (2013) P11003, [[arXiv:1304.5115](#)].
- [29] **DUNE** Collaboration, B. Abi et al., *Experiment Simulation Configurations Approximating DUNE TDR*, [arXiv:2103.04797](#).
- [30] **Hyper-Kamiokande** Collaboration, K. Abe et al., *Physics potentials with the second Hyper-Kamiokande detector in Korea*, *PTEP* **2018** (2018), no. 6 063C01, [[arXiv:1611.06118](#)].
- [31] C. Bronner, *Recent results and future prospects from T2K*", [Talk at the Neutrino 2022, 1st June, 2022](#).
- [32] J. Hartnell, *New results from the NOvA Experiment*", [Talk at the Neutrino 2022, 1st June, 2022](#).
- [33] S. K. A. Moon Moon Devi, Tarak Thakore and A. Dighe, *Enhancing sensitivity to neutrino parameters at INO combining muon and hadron information*, *JHEP* (2014) [[arXiv:1406.3689](#)].
- [34] H. Nunokawa, S. J. Parke, and R. Zukanovich Funchal, *Another possible way to determine the neutrino mass hierarchy*, *Phys. Rev. D* **72** (2005) 013009, [[hep-ph/0503283](#)].
- [35] S. K. Raut, *Effect of non-zero $\theta(13)$ on the measurement of $\theta(23)$* , *Mod. Phys. Lett. A* **28** (2013) 1350093, [[arXiv:1209.5658](#)].
- [36] V. A. Kostelecky and N. Russell, *Data Tables for Lorentz and CPT Violation*, *Rev. Mod. Phys.* **83** (2011) 11–31, [[arXiv:0801.0287](#)].
- [37] **DUNE** Collaboration, R. Acciarri et al., *Long-Baseline Neutrino Facility (LBNF) and Deep Underground Neutrino Experiment (DUNE): Conceptual Design Report, Volume 4 The DUNE Detectors at LBNF*, [arXiv:1601.02984](#).
- [38] **DUNE** Collaboration, B. Abi et al., *Deep Underground Neutrino Experiment (DUNE), Far Detector Technical Design Report, Volume IV: Far Detector Single-phase Technology*, *JINST* **15** (2020), no. 08 T08010, [[arXiv:2002.03010](#)].